Electronic Supplementary Information

Stable Mn(II) Coordination Polymers Demonstrating Proton Conductivity and Quantitative Sensing of Oxytetracycline in Aquaculture

Xu Zhang,[a] Yana Zhang,[a] Xin Li,[a] Jiahui Yu,[a] Weijia Chi,[a] Zikang Wang,[a] Hanwen Zheng,[a] Zhengang Sun*[a], Yanyu Zhu*[a], Chengqi Jiao*[a, b]

[a] School of Chemistry and Chemical Engineering, Liaoning Normal University, Dalian 116029, P. R. China

[b] State Key Laboratory of Fine Chemicals, Dalian University of Technology, Dalian 116024, P. R. China.

E–mail: szg188@163.com, summeryyzhu@163.com, jiaochengqi1989@163.com

CONTENTS:

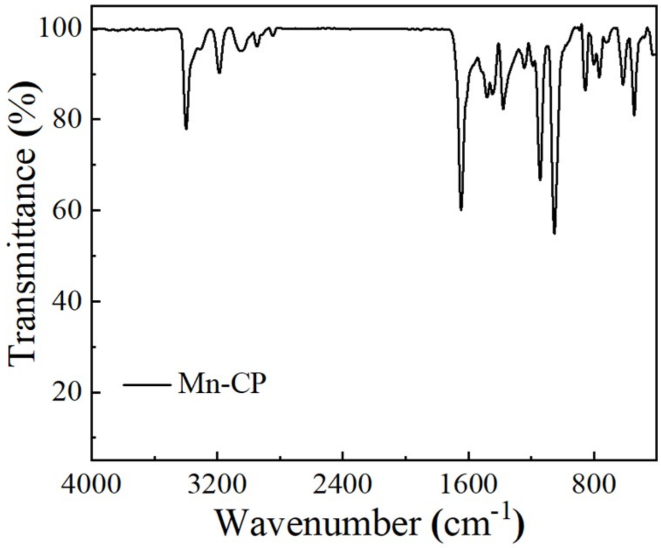

Fig. S1. IR spectrum of **Mn-CP**.

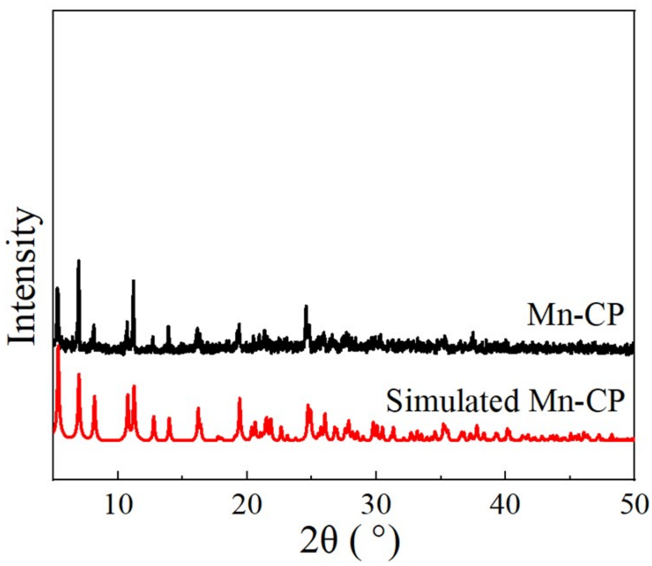

Fig. S2. PXRD pattern of **Mn-CP**.

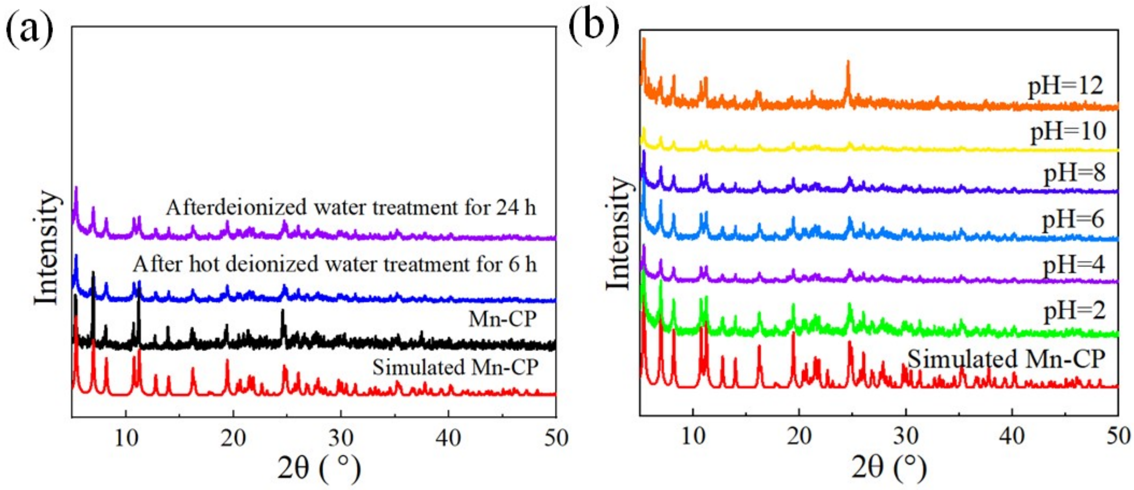

Fig. S3. PXRD patterns of **Mn-CP** soaked in hot deionized water for 6 h and soaked in deionized water for 24 h (a) and soaked in H_2O with different pH for 24 h (b).

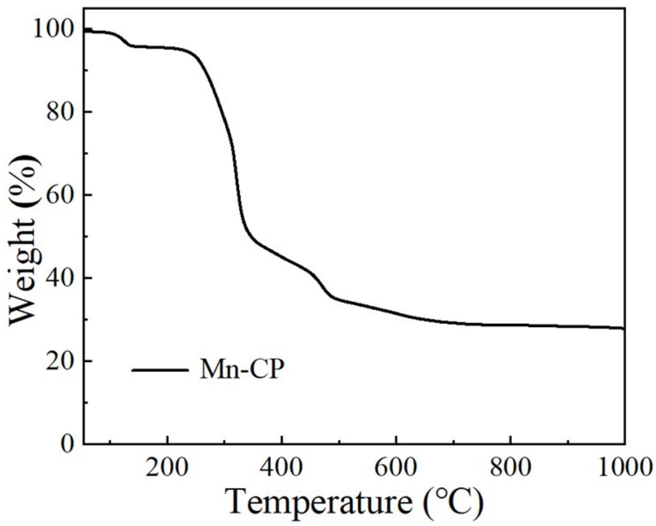

Fig. S4. TG curve of **Mn-CP**.

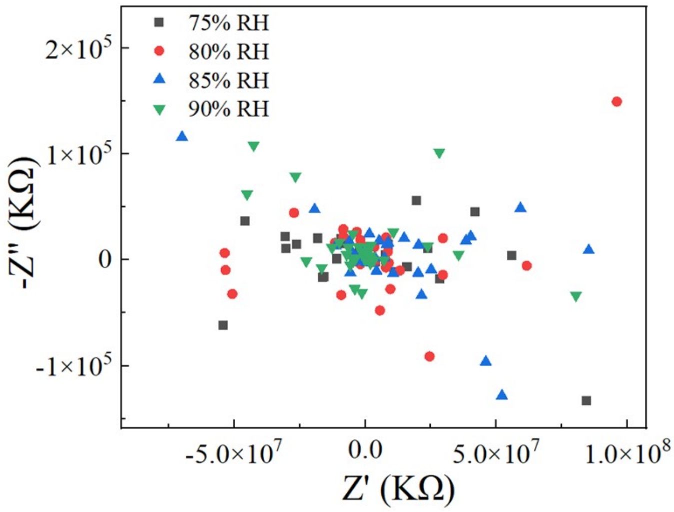

Fig. S5. Nyquist plots of **Mn-CP** at 75-95% RH and 348 K.

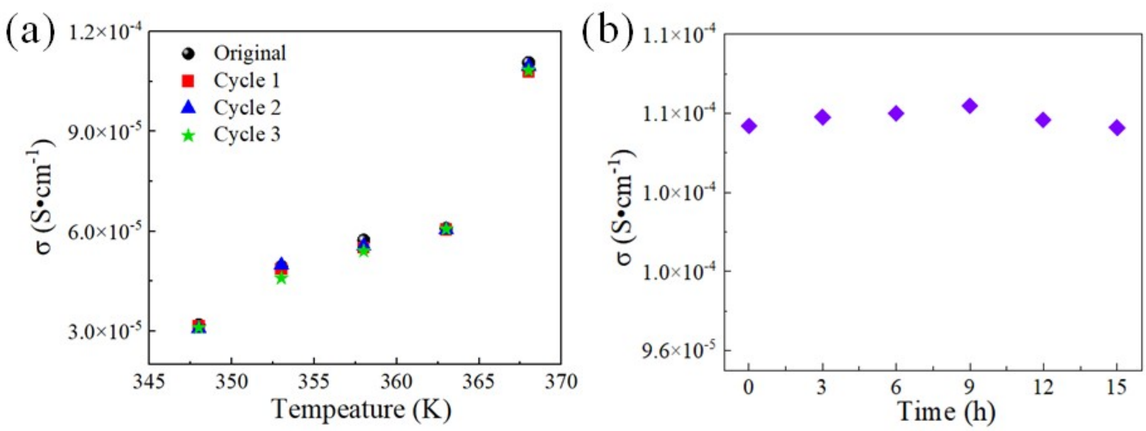

Fig. S6. The recyclable performances of proton conduction of **Mn–CP** under different temperatures (348 – 368 K, 95% RH) (a), and within 15 h (368 K, 95% RH) (b).

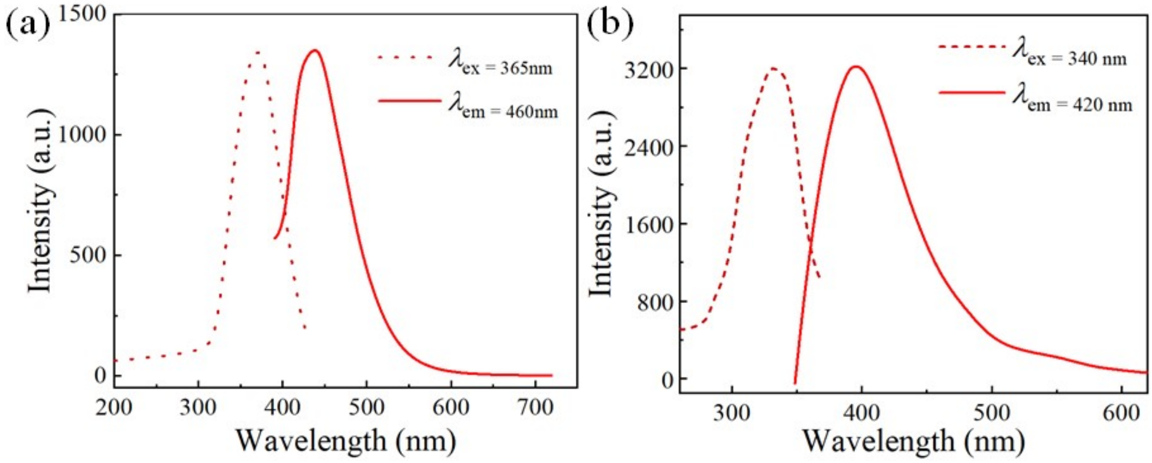

Fig. S7. Solid–state luminescent spectra of H_2L (a) and **Mn-CP** (b).

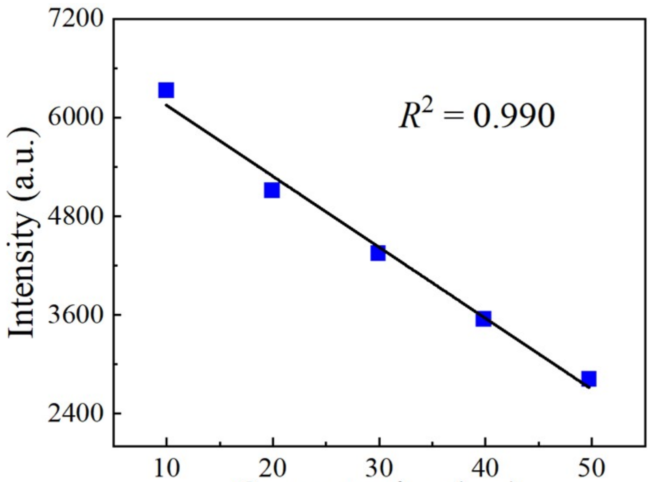

Fig. S8. Plot of the emission intensities of **Mn-CP** *vs* the concentrations of OTC.

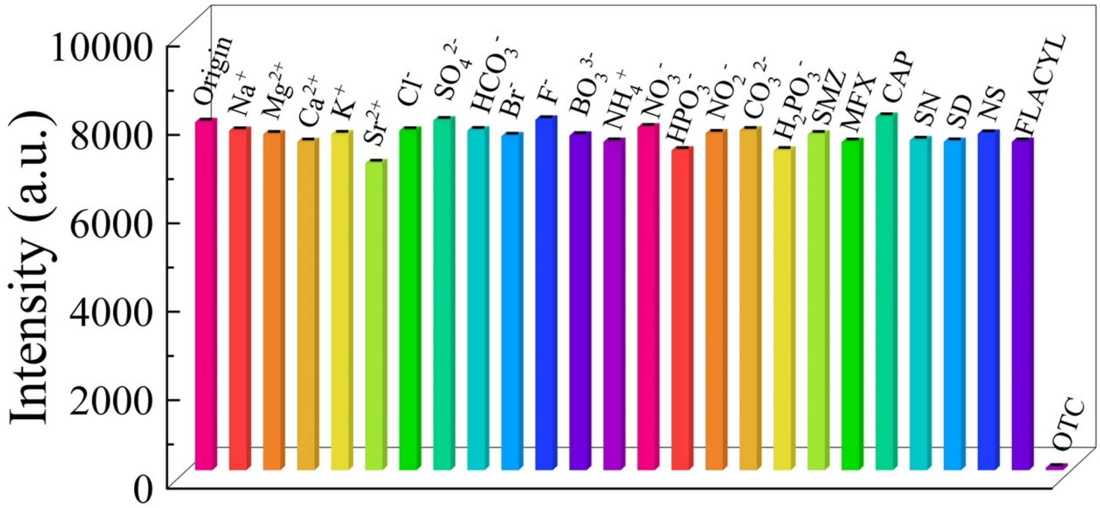

Fig. S9. The luminescent intensities at 413 nm of **Mn–CP** among various substances.

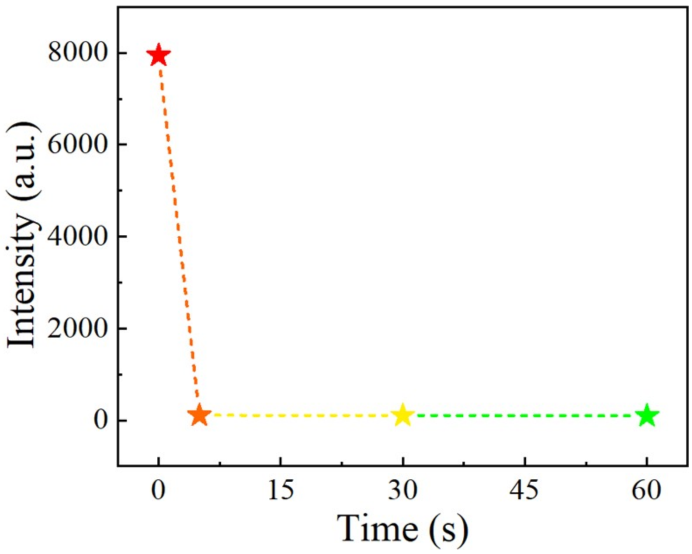

Fig. S10. The luminescent intensities at 413 nm of **Mn-CP** after the addition of OTC at different times

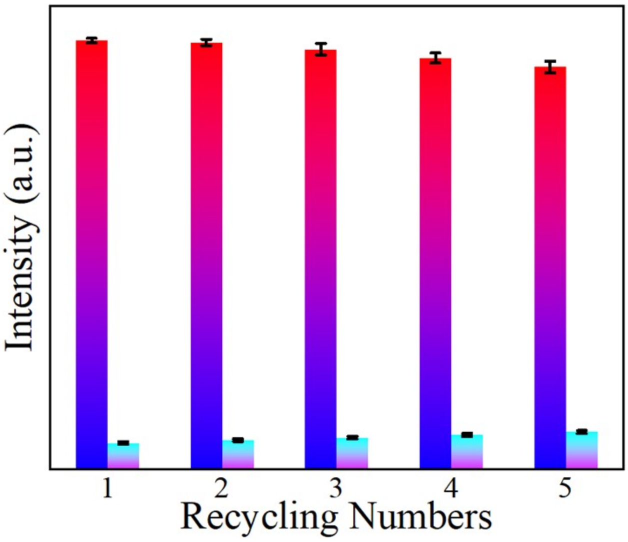

Fig. S11. The recyclable study of **Mn-CP** towards OTC

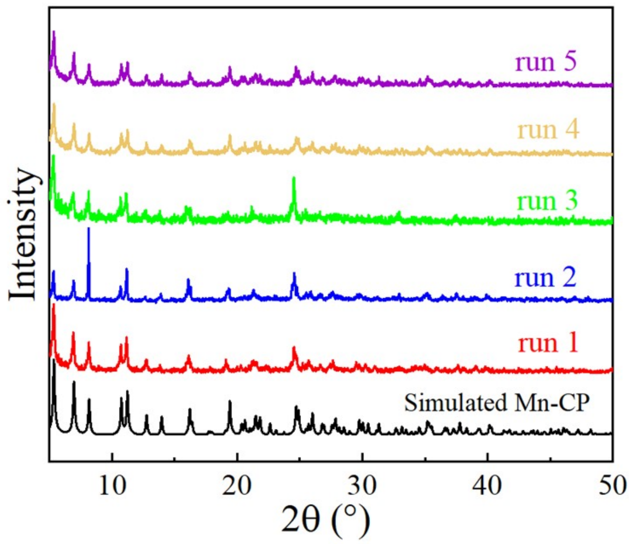

Fig. S12. PXRD patterns of **Mn-CP** after five recycles of sensing for OTC.

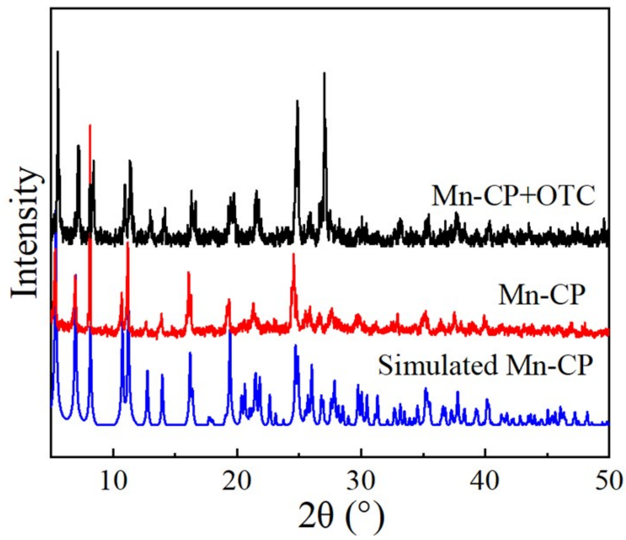

Fig. S13. PXRD patterns of **Mn-CP** before and after detection of OTC.

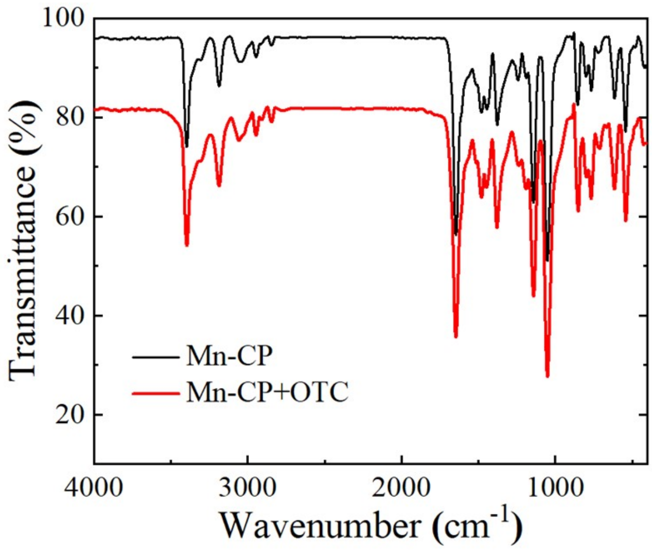

Fig. S14. IR spectra of **Mn-CP** before and after detection of OTC.

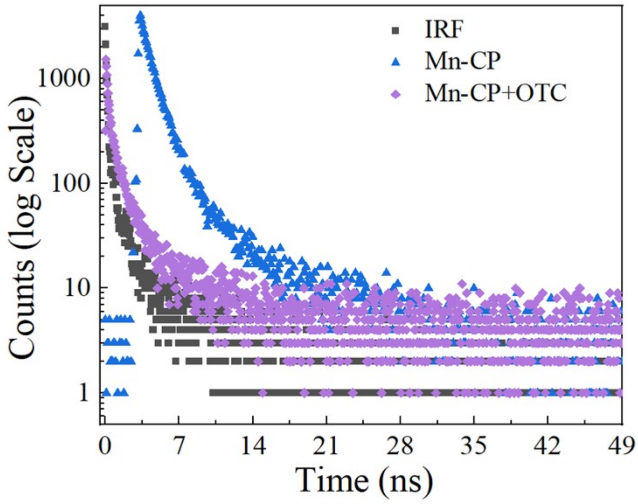

Fig. S15. Emission decay profiles of **Mn-CP** suspensions before and after sensing of OTC.

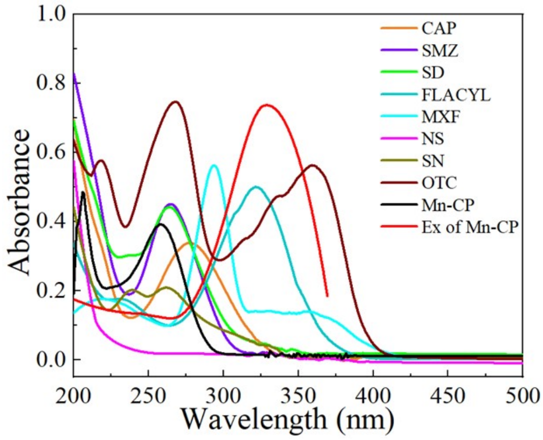

Fig. S16. UV−vis absorption spectra of **Mn-CP**, organic antibiotics and excitation spectrum of **Mn-CP**.

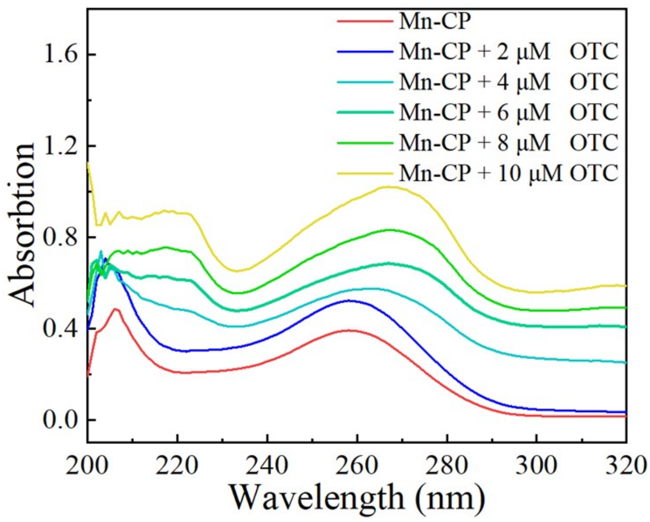

Fig. S17. UV–vis spectra of **Mn-CP** in the presence of various concentrations (0–10 μM) of OTC solutions.

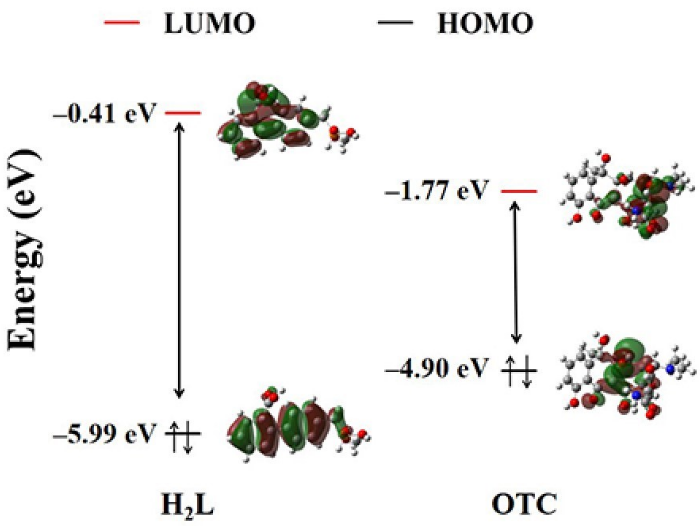

Fig. S18. HOMO and LUMO energy levels of the OTC and the H_2L calculated by density functional theory (DFT) at B3LYP/6–31G* basis set.

Table S1. Crystal data and structure refinements for **Mn-CP**.

Compound	**Mn-CP**
Empirical formula	$C_{15}H_{14}Mn_{0.5}O_5P$
Formula weight	332.70
Crystal system	Orthorhombic
Space group	*P*nna
a/Å	5.1416(6)
b/Å	25.327(3)
c/Å	21.599(3)
α/°	90
β/°	90
γ/°	90
V/Å^3	2812.6(6)
Z	8
ρ_{calc}g/cm^3	1.571
μ/mm^{-1}	5.421
F(000)	1372
Reflections collected	10314
Independent reflections	2516 [R_{int} = 0.0751]
Completeness	100%
Goodness of fit on F^2	1.069
[a]R_1, wR_2 [I>2σ(I)]	0.0617, 0.1473
[a]R_1, wR_2 (all data)	0.0811, 0.1597

[a] $R_1 = \Sigma (|F_0|-|F_C|) / \Sigma |F_0|$; $wR_2 = [\Sigma w (|F_0|-|F_C|)^2 / \Sigma w F_0^2]^{1/2}$

Table S2. Selected bond lengths (Å) and angles (º) for **Mn-CP.**

$Mn1–Mn1^{1}$	3.1634(12)
$Mn1–Mn1^{2}$	3.1634(12)
Mn1–O1	2.092(3)
$Mn1–O1^{3}$	2.092(3)
$Mn1–O2^{4}$	2.175(3)
$Mn1–O2^{1}$	2.289(3)
$Mn1–O2^{5}$	2.175(3)
$Mn1–O2^{6}$	2.289(3)
$Mn1^{1}–Mn1–Mn1^{2}$	108.71(6)
$O1–Mn1–Mn1^{2}$	140.60(9)
$O1–Mn1–Mn1^{1}$	83.39(8)
$O1^{3}–Mn1–Mn1^{2}$	83.39(8)
$O1^{3}–Mn1–Mn1^{1}$	140.60(9)
$O1^{3}–Mn1–O1$	111.31(17)
$O1–Mn1–O2^{4}$	84.80(11)
$O1^{3}–Mn1–O2^{4}$	162.93(11)
$O1^{3}–Mn1–O2^{5}$	96.78(11)
$O1–Mn1–O2^{5}$	85.86(11)
$O1–Mn1–O2^{6}$	96.78(11)
$O1–Mn1–O2^{1}$	162.93(11)
$O1^{3}–Mn1–O2^{1}$	84.80(11)
$O1^{3}–Mn1–O2^{6}$	85.86(11)
$O2^{4}–Mn1–Mn1^{1}$	43.45(8)
$O2^{1}–Mn1–Mn1^{1}$	80.34(8)
$O2^{6}–Mn1–Mn1^{2}$	46.34(7)
$O2^{1}–Mn1–Mn1^{2}$	43.45(8)
$O2^{5}–Mn1–Mn1^{2}$	130.02(9)
$O2^{4}–Mn1–Mn1^{2}$	80.34(8)
$O2^{5}–Mn1–Mn1^{1}$	46.34(7)
$O2^{6}–Mn1–Mn1^{1}$	130.02(9)
$O2^{1}–Mn1–O2^{4}$	79.86(15)
$O2^{5}–Mn1–O2^{4}$	89.79(11)
$O2^{6}–Mn1–O2^{1}$	89.79(11)
$O2^{6}–Mn1–O2^{4}$	86.64(10)
$O2^{5}–Mn1–O2^{1}$	86.64(10)
$O2^{5}–Mn1–O2^{6}$	175.34(16)

Symmetry transformations used to generate equivalent atoms: #1 1–x, 1–y,1–z; #2 –x, 1–y, 1–z; #3 1/2–x, 1–y, +z; #4 3/2–x, 1–y, +z; #5 –1+x, +y, +z; #6 –1/2+x, +y, 1–z.

Table S3. Compositions of proton conductivity with different CPs materials.

Compounds	***σ* (S cm^{-1})**	**conditions**	***E*$_a$ (eV)**	**Ref.**
$(Hdmbpy)[Dy(H_2dobdc)_2(H_2O)]\cdot3H_2O$	1.20×10^{-3}	80 °C-100% RH	0.38	[S6]
$\{[Cd_2(C_2O_4)(2,2'\text{-}bpy)_2(H_2O)_4]\cdot L\cdot3H_2O\}_n$	2.41×10^{-3}	85 °C-98% RH	0.21	[S7]
$\{[Zn_2(1,2,4,5\text{-}BTA)](4,4'\text{-}tmdp)_2]\cdot5H_2O\}_n$	1.09×10^{-4}	100 °C, 98% RH	0.38	[S8]
$\{[Zn_2(1,2,4,5\text{-}BTA)(4,4'\text{-}tmdp)(H_2O)_3]\cdot2.25H_2O\}_n$	1.44×10^{-4}	100 °C, 98% RH	0.32	[S8]
$Cu_4(L)_2(OH)_2(DMF)_2$	7.40×10^{-4}	95 °C-95% RH	1.32	[S9]
Mn–CP	**1.07×10^{-4}**	**95 °C-95% RH**	**1.42**	**This work**
$\{Cd(1,2,4,5\text{-}BTA)_{0.5}\}_n$	1.25×10^{-5}	100 °C, 98% RH	0.40	[S8]
$\{[Cu(pyz)(5\text{-}Hsip)(H_2O)_2]\cdot(H_2O)_2\}_n$	3.50×10^{-5}	65 °C-95% RH	0.35	[S10]
$\{[Zn_3(Htimb)_2(H_2timb)_2(H_2O)_2(ZnW_{12}O_{40})_2]\cdot2H_2O\}_n$	2.32×10^{-5}	85 °C-98% RH	0.52	[S11]
$\{[Ni(Htimb)(H_2O)_3(H_2W_{12}O_{40})_{0.5}]\cdot3H_2O\}_n$	3.38×10^{-5}	85 °C-98% RH	0.16	[S11]
$[Zn(Hssa)(1,4\text{-}bib)\cdot H_2O]_n$	3.45×10^{-5}	60 °C-95% RH	0.28	[S12]
$[Zn_3(ssa)_2(1,4\text{-}bib)_3\cdot4H_2O]_n$	6.26×10^{-6}	60 °C-95% RH	0.35	[S12]
$[Cd_5(TCA)_2(H_2O)_2]\cdot8DMA\cdot16H_2O$	1.45×10^{-6}	80 °C-85% RH	0.74	[S13]
$(Imi)_2[Bi_2(pzdc)_4]\cdot2H_2O$	8.41×10^{-6}	85 °C-95% RH	0.31	[S14]

Table S4. Comparison of the proposed sensor for OTC detection with other methods.

Compounds	**K_{sv} (M^{-1})**	**LOD (nM)**	**Visual detection**	**Ref.**
$2[Zn_2\cdot L(H_2O)_2]$	–	1.21	No	[S15]
Mn–CP	**3.78×10^4**	**4.41**	**Yes**	**This work**
Ag^+/Tb^{3+}@UiO-66-$(COOH)_2$	–	9.1	Yes	[S16]
$2[Cd(H_2L)\cdot(H_2O)_2]$	–	25.4	No	[S15]
BUT–179	2.96×10^5	25.4	No	[S17]
JNU-104	1.52×10^4	29	Yes	[S18]
EuUCBA.	9.755×10^3	118	No	[S19]
Tb-MOF	–	120	Yes	[S20]
Eu-MOF	3.22×10^4	130	Yes	[S21]
BUT–178	8.29×10^4	205	No	[S17]
JNU-205-Eu	2.37×10^4	350	Yes	[S22]

Table S5. Luminescent lifetimes of **Mn–CP** before and after sensing OTC.

Compounds	IRF	τ_{before} (ns)	τ_{after} (ns)
Mn–CP	0.67	2.07	1.82

Reference

S1. F. G. Chen, W. Xu, J. Chen, H. P. Xiao, H. Y. Wang, Z. Y. Chen and J. Y. Ge, Dysprosium(III) Metal–Organic Framework Demonstrating Ratiometric Luminescent Detection of pH, Magnetism, and Proton Conduction, *Inorg. Chem.*, **2022**, *61*, 5388-5396.

S2. B. C. Wang, X. P. Li, B. B. Hao, C. X. Zhang and Q. L. Wang, Dual-Functional Coordination Polymer with High Proton Conductivity and a Low-Detection-Limit Fluorescent Probe, *J. Phys. Chem. B.*, **2021**, *125*, 12627-12635.

S3. G. Q. Shi, H. W. Wang, Q. X. Wang and G. Li, Water-mediated proton conductive properties of three water-stable metal-organic frameworks constructed by pyromellitic acid, *J. Solid. State. Chem.*, **2022**, *307*, 122874.

S4. X. Meng, S. Y. Song, X. Z. Song, M. Zhu, S. N. Zhao, L. L. Wu and H. J. Zhang, A tetranuclear copper cluster-based MOF with sulfonate–carboxylate ligands exhibiting high proton conduction properties, *Chem. Commun.*, **2015**, *51*, 8150-8152.

S5. D. K. Maity, K. Otake, S. Ghosh, H. Kitagawa and D. Ghoshal, Sulfonic Group Functionalized Mixed Ligand Coordination Polymers: Synthesis, Characterization, Water Sorption, and Proton Conduction Studies, *Inorg. Chem.*, **2017**, *56*, 1581-1590.

S6. L. L. Chen, Y. J. Shi, W. W. Wu, J. X. Wang, Y. M. Li, Y. Bai and D. B. Dang, Three new POM-based coordination polymers with 1,3,5-tris(1-imidazolyl)benzene ligand: syntheses, structures and proton conductivity, *CrystEngComm*, **2022**, *24*, 1556-1563.

S7. T. Y. Xu, H. J. Nie, J. M. Li and Z. F. Shi, Highly selective sensing of Fe^{3+}/Hg^{2+} and proton conduction using two fluorescent Zn(ii) coordination polymers, *Dalton Trans.*, **2020**, *49*, 11129-11141.

S8. Y. Shen, X. F. Yang, H. B. Zhu, Y. Zhao and W. S. Li, A unique 3D metal–organic framework based on a 12-connected pentanuclear Cd(ii) cluster exhibiting proton conduction, *Dalton Trans.*, **2015**, *44*, 14741-14746.

S9. M. A. A. Al-Nubi, A. M. Hamisu, A. Ariffin, J. F. Zhang, G. K. H. Shimizu, H. Jo, K. M. Ok and A. C. Wibowo, A new bismuth coordination polymer with proton conductivity and orange-red photoluminescence, *J. Coord. Chem.*, **2021**, *74*, 1810-1822.

S10. F. Sun, H. H. Xie, X. Liu, S. Y. Pang, S. F. Tang and X. L. Xu, Two luminescent phosphonate metal-organic framework as highly efficient and sensitive sensors for the detections of tetracycline antibiotic in aqueous system, *J. Solid. State. Chem.*, **2023**, *322*, 123942.

S11. T. X. Li, Z. X. Chen, Z. S. Zhao and Z. D. Liu, A portable test strip fabricated of luminescent lanthanide-functionalized metal–organic frameworks for rapid and visual detection of tetracycline antibiotics, *Anal. Methods.*, **2023**, *15*, 4459-4466.

S12. L. Liu, Q. Chen, J. Lv, Y. P. Li, K. C. Wang and J. R. Li, Stable Metal–Organic Frameworks for Fluorescent Detection of Tetracycline Antibiotics, *Inorg. Chem.*, **2022**, *61*, 8015-8021.

S13. X. Wu, X. Xiong, J. L. Li, D. Luo, K. Wu, Y. B. Wei, X. Y. Liu, W. G. Lu, D. Li and J. He, An Adenine-Based Biological Metal-Organic Framework as an Efficient Luminescent Sensor for Tetracycline Detection, *Eur. J. Inorg. Chem.*, **2022**, *2022*, e202200278.

S14. J. X. He, H. Q. Yuan, Y. F. Zhong, X. X. Peng, Y. F. Xia, S. Y. Liu, Q. Fan, J. L. Yang, K. Deng, X. Y. Wang and G. M. Bao, A luminescent Eu^{3+}-functionalized MOF for sensitive and rapid detection of tetracycline antibiotics in swine wastewater and pig kidney, *Spectrochim. Acta. A.*, **2022**, *277*, 121252.

S15. C. Y. Zhang, K. R. Lu, L. R. Li, W. Lei, M. Z. Xia and F. Y. Wang, A water-stabilized Tb-MOF can be used as a sensitive and selective fluorescence sensor for the detection of oxytetracycline hydrochloride, *Spectrochim. Acta. A.*, **2023**, 123379.

S16. J. J. Hu, K. L. Xie, T. Z. Xiong, M. M. Wang, H. R. Wen, Y. Peng and S. J. Liu, Stable Europium(III) Metal–Organic Framework Demonstrating High Proton Conductivity and Fluorescence Detection of Tetracyclines, *Inorg. Chem.*, **2023**, *62*, 12001-12008.

S17. K. Wu, X. Y. Liu, Y. L. Huang, M. Xie, X. Xiong, J. Zheng, W. G. Lu and D. Li, Pyrazine functionalization to boost the antenna effect in rare-earth metal–organic frameworks for tetracycline detection, *Inorg. Chem. Front.*, **2022**, *9*, 1714-1721.